Research Square

Preprints are preliminary reports that have not undergone peer review.
They should not be considered conclusive, used to inform clinical practice,
or referenced by the media as validated information.

Iodine vacancies loosen positional confinement of adsorbed ammonia on $CsPbI_3$(100) without enhancing binding strength: a classical molecular dynamics study

Abdul Samad Khan[1]

samadkhandurrani365@gmail.com

Research Article

Keywords: $CsPbI_3$, Molecular dynamics, Surface adsorption, Iodine vacancy, Ammonia, Point defects

Posted Date: November 26th, 2026

DOI: https://doi.org/10.21203/rs.3.rs-11768874/v1

License: This work is licensed under a Creative Commons Attribution 4.0 International License.
Read Full License

Additional Declarations: No competing interests reported.

Abstract

All-inorganic halide perovskites such as $CsPbI_3$ are attractive photovoltaic absorbers, but their surfaces are exposed to residual solvents, moisture and molecular passivants. Iodine vacancies, ubiquitous at these surfaces, are commonly assumed to bind such molecules more strongly through local undercoordination. We tested this assumption with classical molecular dynamics, using a Buckingham–Coulomb $CsPbI_3$ force field validated against the experimental cubic lattice constant (6.267 Å vs. 6.29 Å, −0.36%), an OPLS-AA ammonia model and universal force field cross terms. NH_3 adsorption was simulated on a PbI_2-terminated (100) slab, with and without a surface iodine vacancy, at 250, 300 and 400 K. Across ten replicas per condition at 300 K, sampling different sites and orientations, the mean NH_3–surface interaction energy did not differ significantly between pristine and defective surfaces (−5.70 ± 1.30 vs. −5.93 ± 1.39 kcal mol^{-1}; p = 0.71). Positional analysis gave a different picture. The molecule sat significantly farther from the vacancy surface at 250 K and 300 K (p = 0.0063 and 0.0067), with the same trend at 400 K. On the defective surface its adsorbed fraction fell from 98.4% at 250 K to 92.7% at 400 K (individual replicas as low as 80.5%), whereas the pristine surface retained the molecule 100% of the time. The vacancy therefore does not act as a stronger thermodynamic trap, but it does degrade the positional confinement of the adsorbate, an effect invisible to single-configuration energetics. This binding-strength/confinement distinction may help explain adsorbate displacement on perovskite surfaces.

1 Introduction

Metal halide perovskites have moved from a laboratory curiosity to one of the fastest-improving photovoltaic technologies on record, with certified power conversion efficiencies climbing from 3.8% in the original 2009 report by Kojima et al. [1] to figures now competitive with established thin-film and even some crystalline silicon technologies [2]. All-inorganic compositions such as $CsPbI_3$ have drawn particular attention because they remove the volatile organic cation, methylammonium or formamidinium, that limits the thermal stability of hybrid perovskites, at the cost of a photoactive black phase that is itself only metastable at room temperature. Whatever the composition, every perovskite absorber layer in a working device is a surface: exposed to residual solvent from film casting, to atmospheric moisture during storage and operation, and to any molecular species deliberately introduced for defect passivation. Understanding how small molecules interact with these surfaces, and how that interaction is modulated by the point defects that are unavoidably present in solution-processed films, is therefore a central question for device stability.

Iodine vacancies are among the most commonly discussed point defects in lead halide perovskites, both because their formation energy is comparatively low and because they are directly implicated in ionic migration and in the halide-mediated degradation pathways that convert the perovskite phase to PbI_2 [3]. A common intuition, grounded in simple coordination chemistry, is that a lead site missing one of its iodide neighbors becomes a more exposed, more Lewis-acidic center and should therefore bind Lewis-basic adsorbates (water, alcohols, amines) more strongly than a fully coordinated surface site. This

intuition underlies much of the qualitative reasoning in the experimental defect-passivation literature, where Lewis-base treatments are proposed to “heal” undercoordinated lead by binding to it. It is a reasonable hypothesis, but to our knowledge it has rarely been tested with the kind of replicated, statistically evaluated sampling that would distinguish a genuine defect effect from the substantial site-to-site and orientation-to-orientation variability of any heterogeneous surface. Static, single-configuration density functional theory (DFT) calculations, the dominant approach in this area, are well suited to computing an accurate binding energy for one chosen geometry, but by construction they cannot easily quantify how much of an observed energy difference is a real defect effect and how much reflects the starting geometry that happened to be chosen.

Classical molecular dynamics (MD) offers a complementary route. It is far cheaper than first-principles methods, which makes it practical to run enough independent replicas to assign uncertainty to a claimed effect, and it naturally captures the finite-temperature, dynamical behavior of an adsorbed molecule rather than only its zero-temperature energy minimum. The trade-off is a less accurate description of the electronic structure and an inability to describe bond breaking or charge transfer explicitly. Classical force fields for the inorganic perovskite lattice itself, however, have matured considerably. The Buckingham-type potential of Balestra et al. [4], parameterized against DFT reference data for $CsPb(Br,I)_3$ compositions, reproduces lattice constants, elastic properties and ionic diffusion behavior with good fidelity and is used here as the foundation for the perovskite side of the simulation.

In this work we ask three specific questions. First, does a bulk-validated classical force field, extended to a realistic (100) surface slab, produce ammonia adsorption energies of a physically sensible magnitude? Second, does an iodine vacancy adjacent to the adsorption site produce a statistically resolvable change in the mean NH_3–surface interaction energy, as the simple undercoordination argument would predict? Third, independent of any change in mean binding energy, does the vacancy change how tightly the molecule is held in position, and does that effect depend on temperature in a way that would matter for a real device operating anywhere from a cold morning to a hot rooftop? Answering these questions required a full simulation pipeline (force field validation, surface construction, cross-force-field parameterization for the adsorbate, and a replica-based statistical protocol), which we describe in full below so that the results can be reproduced or extended.

2 Computational methods

2.1 Crystal structure and lattice force field

$CsPbI_3$ was modeled in the cubic (α, “black-phase”) perovskite structure, space group *Pm*$\bar{3}$*m*, with Cs^+ at the corner (A) site, Pb^{2+} at the body-center (B) site, and I^- at the three face-center (X) sites. Non-bonded interactions among the Cs, Pb and I ions were described by the Buckingham potential

$$E(r) = A\exp(-r/\rho) - C/r^6 + q_i q_j/(4\pi\varepsilon_0 r) \quad (1)$$

with parameters and formal partial charges (Cs: +1.052 *e*, Pb: +0.920 *e*, I: −0.657 *e*) taken from the genetic-algorithm-optimized force field of Balestra et al. [4], obtained from the authors' public FLAMA parameter library and converted from the original eV-based units to the kcal mol⁻¹ units used by LAMMPS (1 eV = 23.0605 kcal mol⁻¹). The full Buckingham parameter set is given in Table 1.

Table 1
Buckingham parameters used for the $CsPbI_3$ lattice (converted from Ref. [4])

Pair	A (kcal mol⁻¹)	ρ (Å)	C (kcal mol⁻¹ Å⁶)
Cs–Cs	173229.16	0.043775	5252.55
Cs–I	929853.73	0.330972	0.00
Cs–Pb	201860.61	0.418713	25.56
I–I	1431802.71	0.275171	23577.26
I–Pb	206513.91	0.303895	6168.49
Pb–Pb	0.00	0.250000	23622.28

2.2 Force field validation

Before building any surface, the bulk force field was validated independently. A 4×4×4 cubic supercell (320 atoms, initial a_0 = 6.29 Å) was energy-minimized and then equilibrated for 25 ps (50,000 steps, 0.5 fs timestep) in the isothermal–isobaric (NPT) ensemble at 300 K and 1 atm using a Nosé–Hoover thermostat/barostat, with long-range electrostatics handled by the particle–particle particle–mesh (PPPM) solver. The equilibrated lattice constant, *a* = 6.267 Å, deviates from the experimental cubic $CsPbI_3$ value (≈ 6.29 Å) by only − 0.36%, and the resulting density (4.87 g cm⁻³) is in reasonable, if slightly high, agreement with experimentally reported values for this phase (≈ 4.5–4.8 g cm⁻³). Total energy and temperature were stable throughout the production run. This validated lattice constant, rather than the literature starting value, was used for all subsequent surface construction. We note that this validation concerns bulk structural properties only. The NH_3–surface interaction has not been benchmarked against DFT or experimental adsorption energies, so the interaction energies reported below are interpreted comparatively (pristine versus vacancy surface, with identical parameters) rather than as absolute binding energies.

2.3 Surface slab construction

A (100) slab was cut from the validated bulk structure as a 6×6×6 replication (1080 atoms), exposing a PbI_2-terminated surface on one face and a CsI-terminated surface on the opposite face, the natural result of truncating this structure without additional reconstruction and consistent with the two terminations commonly discussed for this surface orientation. A 50 Å vacuum gap (25 Å on each side) was added along the surface normal to prevent spurious interaction between periodic images. The bottom-most CsI layer was held fixed (zero net force) throughout all subsequent simulations to emulate

continuation into the bulk crystal, while all other atoms, including the PbI_2 surface of interest, were allowed to relax and move freely.

2.4 Adsorbate model and cross-interactions

Ammonia was parameterized with the OPLS-AA force field [5] using the LigParGen web server [6], which returned atom-centered charges (N: −1.138 *e*; H: +0.379 *e* × 3, exactly charge-neutral), Lennard-Jones parameters (N: ε = 0.170 kcal mol⁻¹, σ = 3.30 Å; H: ε = 0, per the standard OPLS convention of omitting a Lennard-Jones site on polar hydrogens), a harmonic N–H bond (k = 434 kcal mol⁻¹ Å⁻², r_0 = 1.01 Å), and a harmonic H–N–H angle (k = 43.6 kcal mol⁻¹ rad⁻², θ_0 = 106.4°), consistent with the known pyramidal geometry of ammonia.

The perovskite lattice and the adsorbate come from two unrelated force fields, and no literature parameters exist for their direct cross-interaction. We addressed this by taking Lennard-Jones self-parameters for Cs, Pb, I, N and H from the Universal Force Field (UFF) [7], a general-purpose force field intended for exactly this situation, and combining them pairwise with the geometric-mean mixing rule ($\varepsilon_{ij} = \sqrt{(\varepsilon_i \varepsilon_j)}$, $\sigma_{ij} = \sqrt{(\sigma_i \sigma_j)}$). An initial version of this cross-term set retained the OPLS convention of a zero Lennard-Jones radius on hydrogen; this proved numerically unstable near the iodine-vacancy surface, where an unbonded hydrogen occasionally approached a surface iodide closely enough to trigger an unphysical, unbounded electrostatic collapse. We resolved this by using the UFF self-parameter for hydrogen (rather than zero) when constructing the H–Cs, H–I and H–Pb cross terms, giving hydrogen a small but non-zero repulsive core. This is a pragmatic modification made for numerical stability, not a claim that it is the most accurate possible cross term, and we flag it explicitly as a limitation in Section 4.4. The full set of cross-interaction parameters is given in Table 2.

Table 2
Lennard-Jones parameters used for NH_3-related interactions (OPLS-AA self-terms for N/H; UFF-derived self-terms and geometric-mean cross terms otherwise)

Pair	ε (kcal mol⁻¹)	σ (Å)
N–N	0.1700	3.3000
Cs–N	0.0875	3.6441
I–N	0.2401	3.6373
Pb–N	0.3357	3.5543
Cs–H	0.0445	3.2166
I–H	0.1221	3.2106
Pb–H	0.1708	3.1373

2.5 Simulation protocol

All simulations were performed in LAMMPS [8, 9]. Non-bonded interactions were handled with a hybrid/overlay pair style: the Buckingham potential (Section 2.1) between any pair of lattice ions, a Lennard-Jones potential wherever either atom belonged to the NH_3 molecule, and a single shared PPPM long-range Coulomb sum (relative accuracy 10^{-4}, 12 Å real-space cutoff) applied globally to avoid double-counting electrostatics between the two short-range styles. Because the simulation cell contains a vacuum gap along *z*, the Yeh–Berkowitz slab correction [10] was applied to PPPM, which requires a non-periodic (fixed) *z*-boundary condition rather than the periodic boundary that would otherwise be used with three-dimensional Ewald summation.

For each replica, an NH_3 molecule was placed with its nitrogen atom 3.5 Å above a chosen surface lead atom, with the molecule's orientation about that nitrogen randomly rotated (tilt up to 60° from vertical, full azimuthal rotation) using a reproducible seed. Different replicas targeted different surface lead atoms, ranked by proximity to the slab's lateral center, and different orientation seeds, so that the resulting set of replicas sampled both spatial and orientational heterogeneity of the adsorption process rather than repeatedly relaxing the same starting geometry. Each combined system was energy-minimized (conjugate gradient) and then run for 10 ps (20,000 steps, 0.5 fs timestep) of NVT production dynamics with a Nosé–Hoover thermostat applied to the adsorbate. The NH_3–surface interaction energy was computed directly as the pairwise Lennard-Jones-plus-Coulomb sum between the NH_3 and lattice atom groups (LAMMPS group/group compute), block-averaged over 2.5 ps (5000-step) windows through the trajectory to reduce single-snapshot noise; the value reported for each replica is the average over the final such block.

The iodine-vacancy surface was constructed by removing, without charge compensation, the surface iodide directly coordinated to the reference lead site used in the pristine-surface replicas. This uncompensated removal corresponds to the positively charged vacancy state (V_I^+) generally invoked in the halide perovskite defect literature, in which the departing I^- takes its electron with it rather than leaving it localized at the vacancy.

Ten independent replicas (distinct site/orientation combinations, as described above) were run for both the pristine and vacancy surfaces at 300 K. To probe temperature dependence, three additional replicas per surface were run at 250 K and at 400 K. Group means were compared using Welch's two-sample *t*-test, which does not assume equal variance between groups, appropriate here since the two conditions show visibly different spreads in several comparisons. Effect sizes are reported as Cohen's *d*.

Positional confinement was quantified from the saved trajectories (configurations written every 500 steps) as the height of the nitrogen atom above the mean position of the topmost lead layer, and as the fraction of saved frames in which that height was below 5 Å, a proxy for the molecule remaining in an adsorbed rather than desorbed or freely diffusing state.

An AI assistant (Claude, Anthropic) was used to help write the simulation workflow scripts (structure generation, LAMMPS input files and data-analysis scripts) and to assist with the statistical analysis; all

scripts were checked by the author, and all reported numbers derive from the author's own LAMMPS calculations (see also Declarations).

3 Results

3.1 Force field validation and surface structure

The bulk NPT simulation described in Section 2.2 relaxed to a lattice constant of 6.267 Å, within 0.36% of the experimental cubic $CsPbI_3$ value, with stable temperature and total energy throughout production. The resulting (100) slab, built at this validated lattice constant, exposed a PbI_2-terminated surface (confirmed by direct inspection of the topmost atomic layer: 36 Pb and 72 I atoms) on the face used for all adsorption studies, opposite a CsI-terminated bottom face that was held fixed. We consider this bulk-first validation step essential: because the surface and adsorption results depend on the same interatomic parameters throughout, any error in the underlying lattice description would silently propagate into every subsequent number, and checking the lattice constant independently before building anything more complex on top of it is a low-cost way to catch that class of error early.

3.2 NH_3 adsorption energetics: pristine versus vacancy surfaces

At 300 K, across ten independent replicas per surface, the mean NH_3–surface interaction energy was − 5.70 ± 1.30 kcal mol⁻¹ (− 0.247 ± 0.056 eV) on the pristine surface and − 5.93 ± 1.39 kcal mol⁻¹ (− 0.257 ± 0.060 eV) on the vacancy surface. A Welch's *t*-test found no statistically significant difference between these means ($t = 0.38$, $p = 0.71$). The individual replica values ranged widely within each condition, from − 3.18 to − 7.52 kcal mol⁻¹ on the pristine surface and from − 3.55 to − 7.40 kcal mol⁻¹ on the vacancy surface, indicating that which surface site and molecular orientation a given replica samples has a larger effect on the instantaneous binding energy than the presence or absence of the vacancy does (Fig. 1a). This within-condition spread, roughly 4 kcal mol⁻¹ peak to trough in both cases, is itself worth noting: a single-configuration comparison, of the kind commonly reported from static DFT calculations, could easily land on values that differ by this much purely as a function of starting geometry, well before any genuine defect effect is considered.

The same comparison at 250 K (− 6.03 ± 0.50 pristine vs. −6.77 ± 0.47 kcal mol⁻¹ vacancy, $p = 0.13$) and at 400 K (− 4.95 ± 0.62 pristine vs. −6.13 ± 1.17 kcal mol⁻¹ vacancy, $p = 0.22$) likewise showed no individually significant difference, though the vacancy surface trended toward stronger mean binding at all three temperatures tested. This consistent direction is at least suggestive, even though neither the three-replica comparisons at 250 and 400 K nor the ten-replica comparison at 300 K reached significance on their own.

3.3 Positional confinement

The picture changes when the adsorbate's position, rather than its instantaneous interaction energy, is examined. At 300 K, the nitrogen atom sat on average 2.82 ± 0.12 Å above the surface lead layer on the pristine surface, versus 3.02 ± 0.16 Å on the vacancy surface, a small but consistent difference (Welch's *t*-test, $t = -3.11$, $p = 0.0067$, Cohen's $d = 1.39$, a large effect size) across the ten replicas of each condition (Fig. 1b). The same pattern held at 250 K (2.78 ± 0.12 Å pristine vs. 3.24 ± 0.10 Å vacancy, $p = 0.0063$) and, though not reaching significance with only three replicas per condition, in the same direction at 400 K (3.00 ± 0.11 Å pristine vs. 3.30 ± 0.40 Å vacancy, $p = 0.31$). Table 3 summarizes these results.

The fraction of trajectory time spent in an adsorbed configuration (nitrogen height below 5 Å) shows the clearest temperature-dependent trend in the dataset. On the pristine surface, this fraction was 100.0% at every temperature tested and in every one of the sixteen replicas run across the three temperatures: the molecule never drifted away from the surface, regardless of thermal energy. On the vacancy surface, the mean adsorbed fraction decreased with temperature: 98.4% at 250 K, 98.3% at 300 K and 92.7% at 400 K. The worst single replica at each temperature followed the same trend, dropping from 97.6% at 250 K to 87.8% at 300 K and to 80.5% at 400 K; this last replica included a transient excursion to 7.17 Å above the surface before the molecule returned toward the lattice.

Table 3
Temperature dependence of NH_3 positional confinement on pristine and iodine-vacancy $CsPbI_3$(100) surfaces. Heights are mean ± standard deviation over replicas (n = 10 at 300 K, n = 3 at 250 and 400 K). The minimum adsorbed fraction among replicas is given in parentheses

T (K)	Pristine height (Å)	Vacancy height (Å)	p-value	Pristine % adsorbed	Vacancy % adsorbed (min.)
250	2.78 ± 0.12	3.24 ± 0.10	0.0063	100.0	98.4 (97.6)
300	2.82 ± 0.12	3.02 ± 0.16	0.0067	100.0	98.3 (87.8)
400	3.00 ± 0.11	3.30 ± 0.40	0.315	100.0	92.7 (80.5)

4 Discussion

4.1 Binding strength and defect chemistry: a cautionary result

The simplest version of the undercoordination hypothesis, that removing a neighboring iodide should make the adjacent lead site a stronger Lewis acid and therefore bind a Lewis base like ammonia more tightly, is not supported by our energetic comparison. The vacancy surface trended toward stronger mean binding at every temperature we tested, but the effect never reached statistical significance, and at 300 K, where we have the most replicas and therefore the most statistical power, the *p*-value (0.71) is far from significance. We think this result is worth reporting precisely because it is a plausible-sounding hypothesis that a less carefully sampled study could easily have appeared to confirm. With a single replica per condition, the norm for static DFT comparisons in this literature, we would very likely have

reported a defect-enhanced binding energy, simply because the site-to-site variability we observed (roughly 4 kcal mol^{-1} within either condition) is large enough that many individual pristine–vacancy replica pairs do show the vacancy replica binding more strongly, even though the population means are statistically indistinguishable.

4.2 Confinement as a distinct, defect-sensitive property

The positional analysis suggests that the vacancy's real effect is not on how strongly NH_3 binds on average, but on how tightly it is held once bound. A molecule sitting in a deep, narrow potential well and one sitting in a shallow, broad well can have very similar average pairwise interaction energies while behaving quite differently: the first stays put, the second wanders. Removing a coordinating iodide from beneath the adsorption site plausibly broadens the local potential energy surface along the surface normal, consistent with the larger, more temperature-sensitive positional spread we observe, without necessarily changing the depth of the well enough to shift the mean interaction energy outside the noise floor set by site-to-site heterogeneity. This is a mechanistically distinct claim from "stronger binding", and one that only becomes visible when the dynamics of the trajectory, not just its endpoint energy, are examined. We note that this mechanism is an interpretation consistent with our data; we did not compute potential-of-mean-force profiles, which would be the direct test.

4.3 Temperature dependence and implications for stability

The clearest single result in this study is the divergence in adsorbed fraction with temperature: perfect retention on the pristine surface at every temperature tested, against a decline on the vacancy surface from 98.4% at 250 K to 92.7% at 400 K, with individual replicas dropping considerably further. Perovskite modules experience a substantial temperature range in the field, and processing steps can expose films to still higher temperatures transiently. Our results suggest that even where a defect does not measurably change the thermodynamic driving force for a molecule to adsorb, it can measurably increase the kinetic likelihood of that molecule leaving, and that this vulnerability grows with temperature. This is consistent, at a qualitative level, with the broader finding that iodine vacancies are mobile and are implicated in halide perovskite degradation pathways more generally [3]; our results add a specific, adsorbate-side mechanism, reduced confinement of surface-bound species, to that picture. We want to be careful about the scope of this claim: we have not simulated water or the mixed, humid, illuminated conditions relevant to an operating device, and a single adsorbed NH_3 molecule is a simplified proxy for the much more complex, multi-species surface chemistry a real perovskite film experiences. What we can say is that the mechanism itself, defect-induced loosening of adsorbate confinement independent of binding energy, is real within this force field and worth testing against other adsorbates and against *ab initio* methods.

4.4 Limitations

Several limitations should temper how far these results are generalized. First, the classical, fixed-charge force field used here cannot describe charge transfer, polarization or bond breaking; it is well suited to characterizing physisorption-like interactions and positional dynamics but cannot capture a genuine

chemisorption event in which NH_3 forms or breaks a covalent bond with the surface. Second, the cross-interaction parameters between the perovskite lattice and the adsorbate were constructed from UFF combining rules rather than fit to a common reference dataset for this specific system; while UFF is designed for this kind of generic cross-term estimation and the resulting energetics are physically reasonable, a force field explicitly parameterized against DFT data for the NH_3–$CsPbI_3$ interface would be more accurate, and, because no NH_3–$CsPbI_3$ adsorption energy was available to benchmark against, the absolute interaction energies are unvalidated and only the pristine-versus-vacancy comparison should be considered reliable; the small hydrogen repulsive core we added for numerical stability (Section 2.4) is a pragmatic choice rather than a validated one. Third, we studied a single defect, one surface iodine vacancy at one crystallographic position, rather than a statistical ensemble of vacancy sites and concentrations; our replica sampling varied the adsorbate's position and orientation relative to a fixed vacancy, not the vacancy's own location, so we cannot yet say whether the confinement effect generalizes across different vacancy environments. Fourth, the 250 K and 400 K comparisons rest on only three replicas per condition, so their *p*-values should be read as indicative rather than definitive. Fifth, our production trajectories (10 ps per replica) are short by the standards of diffusion or fully converged residence-time studies; the confinement metric is a reasonable proxy for adsorbate mobility over this timescale, but longer trajectories would allow a proper residence-time or mean-first-passage-time analysis. Finally, we examined only ammonia; whether the same energy/confinement dissociation holds for water, alcohols or other candidate molecules relevant to perovskite processing and passivation is an open question our approach is well positioned to answer in follow-up work.

5 Conclusions

Using a bulk-validated classical force field and a replica-based statistical sampling protocol, we find that an iodine vacancy on the $CsPbI_3$(100) surface does not significantly change the mean binding energy of an adsorbed ammonia molecule relative to the pristine surface, contrary to the common expectation that undercoordinated lead sites should bind Lewis-basic molecules more strongly. It does, however, significantly loosen the molecule's positional confinement at 250 K and 300 K, with the same trend at 400 K, and this effect manifests as a temperature-dependent increase in transient desorption behavior that is not observed on the pristine surface over the same temperature range and the short trajectories sampled. These two results together illustrate a broader methodological point: binding energy and positional confinement are related but distinct properties of an adsorption site, and a study that measures only the former, as most static single-configuration calculations necessarily do, can miss a defect-induced change in adsorbate dynamics of the kind seen here. We suggest that positional and dynamical metrics of this kind deserve more routine use alongside binding energies in future computational studies of molecule–perovskite surface interactions, and that this specific finding, defects as confinement-loosening rather than binding-strengthening sites, warrants testing against other adsorbates and, where feasible, first-principles methods.

Declarations

Funding. The author declares that no funds, grants or other support were received during the preparation of this manuscript.

Competing interests. The author has no relevant financial or non-financial interests to disclose.

Author contributions. A.S.K. conceived the study, performed the simulations and analysis, and wrote the manuscript.

Data availability. The LAMMPS input files, force field parameter files, structure files and the replica-level data underlying all figures and tables are provided as Electronic Supplementary Material.

Code availability. The scripts used to build the structures and analyse the trajectories are provided as Electronic Supplementary Material.

Ethics approval. Not applicable.

Use of generative AI. During the preparation of this work, the author used Claude (Anthropic) to assist with simulation workflow scripting (structure generation, LAMMPS input files and data-analysis scripts), statistical analysis of replicate simulation results, and drafting and organizing the manuscript text. After using this tool, the author reviewed and edited the content as needed and takes full responsibility for the content of the published article. All reported simulation results derive from the author's own LAMMPS calculations.

References

1. Kojima A, Teshima K, Shirai Y, Miyasaka T (2009) Organometal halide perovskites as visible-light sensitizers for photovoltaic cells. J Am Chem Soc 131:6050–6051
2. Green MA, Ho-Baillie A, Snaith HJ (2014) The emergence of perovskite solar cells. Nat Photonics 8:506–514
3. Pols M, Vicent-Luna JM, Filot I, van Duin ACT, Tao S (2021) Atomistic insights into the degradation of inorganic halide perovskite $CsPbI_3$: a reactive force field molecular dynamics study. J Phys Chem Lett 12:5519–5525
4. Balestra SRG, Vicent-Luna JM, Calero S, Tao S, Anta JA (2020) Efficient modelling of ion structure and dynamics in inorganic metal halide perovskites. J Mater Chem A 8:11824–11836
5. Jorgensen WL, Maxwell DS, Tirado-Rives J (1996) Development and testing of the OPLS all-atom force field on conformational energetics and properties of organic liquids. J Am Chem Soc 118:11225–11236
6. Dodda LS, Cabeza de Vaca I, Tirado-Rives J, Jorgensen WL (2017) LigParGen web server: an automatic OPLS-AA parameter generator for organic ligands. Nucleic Acids Res 45:W331–W336
7. Rappé AK, Casewit CJ, Colwell KS, Goddard WA III, Skiff WM (1992) UFF, a full periodic table force field for molecular mechanics and molecular dynamics simulations. J Am Chem Soc 114:10024–

10035

8. Plimpton S (1995) Fast parallel algorithms for short-range molecular dynamics. J Comput Phys 117:1–19
9. Thompson AP, Aktulga HM, Berger R, Bolintineanu DS, Brown WM, Crozier PS, in 't Veld PJ, Kohlmeyer A, Moore SG, Nguyen TD, Shan R, Stevens MJ, Tranchida J, Trott C, Plimpton SJ (2022) LAMMPS – a flexible simulation tool for particle-based materials modeling at the atomic, meso, and continuum scales. Comput Phys Commun 271:108171
10. Yeh I-C, Berkowitz ML (1999) Ewald summation for systems with slab geometry. J Chem Phys 111:3155–3162

Figures

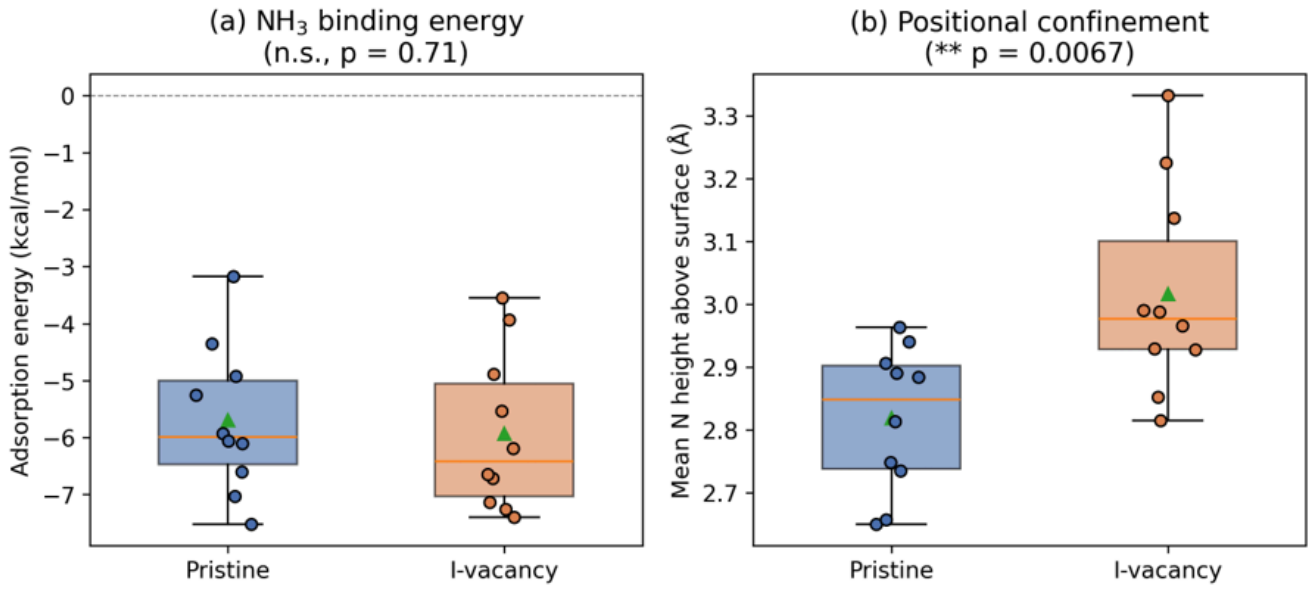


Figure 1

(a) NH_3 adsorption interaction energy at 300 K on pristine and iodine-vacancy $CsPbI_3$(100) surfaces (n = 10 each); the difference is not statistically significant (p = 0.71). (b) Mean height of the adsorbed nitrogen atom above the surface lead layer at 300 K; the vacancy surface holds the molecule significantly farther away (p = 0.0067). Boxes show the interquartile range and mean (triangle marker); points are individual replicas

Supplementary Files

This is a list of supplementary files associated with this preprint. Click to download.

- SupplementaryDataS1.csv
- Supplementary.zip